

Precise Angle Control of BLDC Motor Driven Multi Channel Electromechanical Actuator Base on ADRC Method

Xiong Chen¹, Aitian Yan¹, Yebing Cui², Jian Zheng²

¹School of Mechanical Engineering, Nanjing University of Science and Technology, Nanjing, 210094, China

²Control Technology Institute of SAST, Shanghai 200235, China

Keywords: Electromechanical actuator, brushless dc motor, active disturbance rejection control, extended state observer, time-optimal control.

Abstract. In this paper modeling, simulation and control of multichannel electromechanical actuator (EMA) for tactical missiles with permanent magnet brushless dc motor (BLDC) were investigated. To improve performances of the system, an extended state observer-based time-optimal control (ESO-TOC) is proposed in this paper, which based on active disturbance rejection control (ADRC). Total disturbance is estimated by an extended state observer, and the nonlinear system is compensated as a linear one. Time-optimal control is used to realize accurate angle motions with minimal time. Simulations and experimental setup are used to demonstrate the effectiveness of the proposed control method. The performance of PID control is compared to the ESO-TOC control in simulation and ESO-TOC control is robust to large parameter variations of 50%. The experimental results show close agreement with the simulation results. The proposed method proved effective by achieving a transient time of 12.5 ms in 5 degree and the bandwidth of the EMA system could achieve 10 Hz, and also good positioning performance has been achieved in the presence of both model uncertainties and external disturbances.

Introduction

With the development of the new kinds of permanent magnetic materials and the technology of drive circuits, more and more electromechanical actuators have been used in aerospace industry [1]. Potential benefits of using EMAs include increased reliability, reduced weight and volume of the integrated power and actuation system, and decreased maintenance requirements. Moreover, EMAs sourced by Lithium ion battery power packs contribute to SRM “instant readiness” [2] .Furthermore, future evolutions of “near zero torque” flex-seal designs should decrease TVC power requirements [3].

However, in the flight of a spacecraft there are some uncertainties [4] and lead to challenges to the control of EMA system.A variety of control methods for EMA have been investigated [5]. The feedback control algorithms mainly include sensorless control [6], [7], nonlinear adaptive robust control [8], Lyapunov function based control [9], and flatness based control, robust synthesized control [5]. Some optimization schemes based on the modern intelligent algorithm are proposed for normal PID[10].However, traditional control schemes have considerable limitations in achieving high bandwidth and robustness for the EMAs of the tactical missiles, since most of the disturbances and nonlinearities could not be modeled accurately.

This paper is organized as follows. Section 2 describes the structure and dynamical model of the EMA aerial rudder system. In section 3, the controller design and controller parameters optimization of the EMA system is proved, Section 4 shows the simulation model and two controllers are compared. Section 5 shows experimental setup and experimental results are compared and discussed.

Structure and Mathematical Model of EMA Aerial Rudder System

Structure of EMA Aerial Rudder System. EMA aerial rudder control system, considered here, is the control of the missile using four channel aerial rudders. The four channel aerial rudders configuration is presented in Fig. 1.

By deflecting them, moments are generated about the center of mass, which in turn rotate the airframe. The missile autopilot sends roll, pitch, and yaw commands (δ_r , δ_y and δ_p) to the EMA aerial rudder control system. Before they can be utilized, they have to be separated into individual aerial rudder commands, i.e. angles δ_i , where $i= 1,2, 3,4$. Each actuator module can convert the reference aerial rudder command into an actual surface deflection and requires tight, independent position control of the surface deflection , usually less than $\pm 25^\circ$.

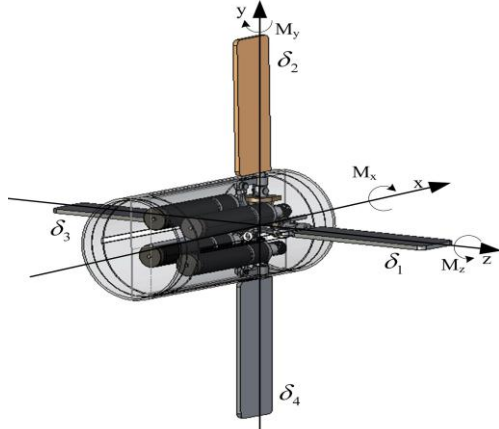


Fig. 1. Schematic structure of EMA aerial rudder system

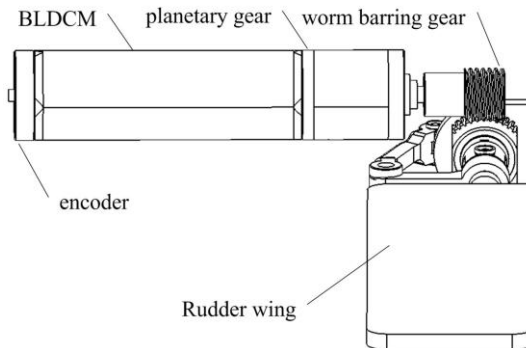


Fig. 2. Schematic illustration of the single EMA.

Mathematical model of EMA. In general, computing the practical output angle involves a large volume of data and is therefore a complex undertaking [11]. According to schematic illustration of the single EMA system shown in the Fig. 2, the construct parts of the system can be modeled as following

Firstly, the three phase voltage equations in a matrix form of the BLDCM under ideal condition can be simplified as

$$U = L \frac{di}{dt} + ri + K_e \omega \quad (1)$$

where, U is the terminal voltage; r is the equivalent terminal resister phase to phase; i is the phase current; L is the equivalent phase inductance; K_e is the back electromotive force constant; ω is the motor Angular velocity. Secondly, the mechanical equation of BLDC can be given as below.

$$T_e - T_l = J \frac{d^2\theta}{dt^2} \quad (2)$$

$$T_e = K_t \cdot i \quad (3)$$

$$\frac{d\theta}{dt} = \omega \quad (4)$$

where, T_e is the electromagnetic torque, T_l is the load torque, J is the whole inertia of the EMA's mechanical working system converting to the motor shaft, θ is the motor mechanical angular. K_t is the torque coefficient. The value of T_l can be assumed zero. According to Eqs.(1)- (4), the transfer function of BLDCM can be derived:

$$\frac{\theta(s)}{u(s)} = \frac{K_t}{s(JLs^2 + Jrs + K_t K_e)} \quad (5)$$

Finally, taking the moderating ratio of the gears into account, the ratio of output angle to the control voltage is

$$\frac{\delta(s)}{u(s)} = \frac{1/(K_e S_i)}{s(Q_e T_m s^2 + T_m s + 1)} \quad (6)$$

After all, Eq. (6) is the EMA system's transfer function , which means the system is third order and should adopt third order ADRC to control the EMA system. In order to simplify design procedure of the controller, the EMA system could be translated into a first-order system and a second-order system in series, since most of the disturbances and nonlinearities could not be modeled accurately.

Controller Design and Controller Parameters Optimization

Consider the following nonlinear second-order plant,

$$\begin{cases} \dot{x}_1 = x_2 \\ \dot{x}_2 = f(x_1, x_2, d(t), t) + b \cdot u \\ y = x_1 \end{cases} \quad (7)$$

where y is the output to control, x_1, x_2 are state variables, u is the control input, b is the system parameter, and $f(x_1, x_2, d(t), t)$ denotes the total disturbance which is nonlinear. The objective is to synthesize a control input u so that the output y gets to the desired point y_d as quickly and accurately as possible in spite of the total disturbance.

ESO. The main role of the ESO is to estimate total disturbance, and its discrete-timeform for second-order plant Eq. (8) with sampling period h is.

$$\begin{cases} e = z_1(k) - y(k) \\ z_1(k+1) = z_1(k) + h \cdot [z_2(k) - \beta_{01} \cdot e] \\ z_2(k+1) = z_2(k) + h \cdot [z_3(k) - \beta_{02} \cdot fal(e, 0.5, \delta) + b \cdot u(k)] \\ z_3(k+1) = z_3(k) - h \cdot \beta_{03} \cdot fal(e, 0.25, \delta) \end{cases} \quad (8)$$

More details can be found in [11].To compensate the total disturbance in real time and therefore the original nonlinear system Eq.(7) is linearized as

$$\begin{cases} \dot{x}_1 = x_2 \\ \dot{x}_2 = u_0 \\ y = x_1 \end{cases} \quad (9)$$

where u_0 is the intermediate control variable, which can be determined by

$$u_0 = -r \cdot \text{sgn}[x_1 - y_d + (x_2 \cdot |x_2|)/(2r)] \quad (10)$$

TOC. The control input Eq. (10) will cause chattering because of the sign function $\text{sgn}(s)$.A novel solution $u_0 = fhan(x_1 - y_d, x_2, r, h_0)$ in[11]is used to achieve TOC while restraining the chattering effectively, which is described as

$$fhan(x_1 - y_d, x_2, r, h_0) = \begin{cases} -r \cdot \text{sgn}(\alpha), |\alpha| > d \\ -r \cdot (\alpha / d), |\alpha| \leq d \end{cases} \quad (11)$$

Control effects of the three solutions are compared in Fig.3, which is implemented in MatLab/Simulink.

Parameters are chosen as: $(h_0, r, \rho, y_d) = (0.0002, 800, 0.001, 0.032)$.

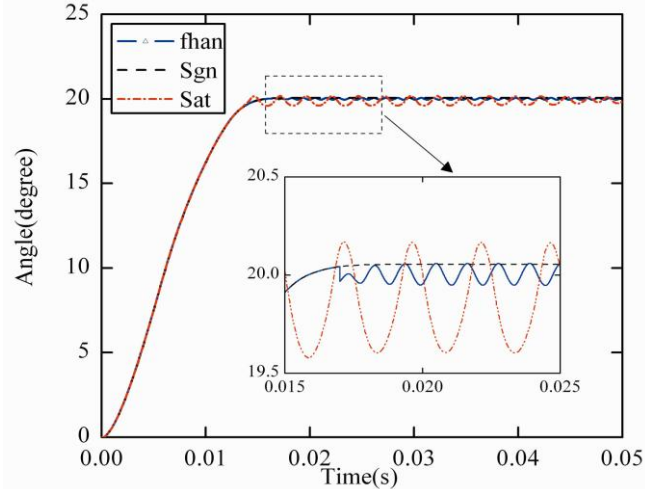


Fig. 3. Control effect comparisons of three TOC solutions.

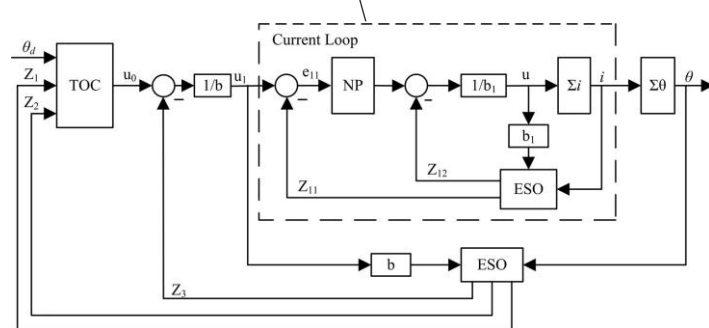


Fig. 4. Fast and precise angle motion control system of EMA.

Fast and Precise Angle Motion Control System. The proposed fast and precise angle motion control system of EMA consists of current and position loops, which is illustrated in Fig.4. ESO-TOC is implemented in the position loop since mechanical dynamics of the EMA is a second-order system, and states x_1 and x_2 are estimated by z_1 and z_2 . u_1 acts as a pseudo control variable calculated by ESO-TOC and the role of the current loop is to make i track u_1 quickly and accurately. Since electrical dynamics of the EMA is a first-order system, ESO in the current loop is established as

$$\begin{cases} e = z_{11}(k) - i(k) \\ z_{11}(k+1) = z_{11}(k) + h_1 \cdot [z_{12}(k) - \beta_{11} \cdot e + b_1 \cdot u(k)] \\ z_{12}(k+1) = z_{12}(k) - h_1 \cdot \beta_{12} \cdot fal(e, 0.5, \delta_1) \end{cases} \quad (12)$$

where z_{11} is the estimate of i , z_{12} is the estimate of the total disturbance acting on the electrical subsystem such as parameter variations, h_1 is the sampling period of the current loop and b_1 is a system parameter.

Comparison simulations of different types of controllers. The proposed controller has been compared with a tuned double closed loop proportional-integral-derivative (PID) controller (a position loop and a current loop) in simulation. As well known, the rapidity, precise, stability and robustness are the key characters of the control system. Comparative simulations are implemented on the EMA using Matlab /Simulink.

Response with Varying Reference Inputs. Fig. 5 shows the system response with respect to varying reference EMA's output angle θ . The reference EMA's output angle θ are step signals and are set to $5, 10, 15^\circ$ respectively.

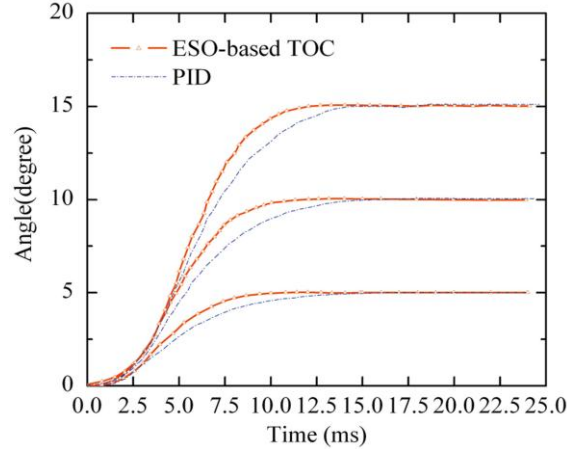


Fig. 5. System step response with various reference inputs.

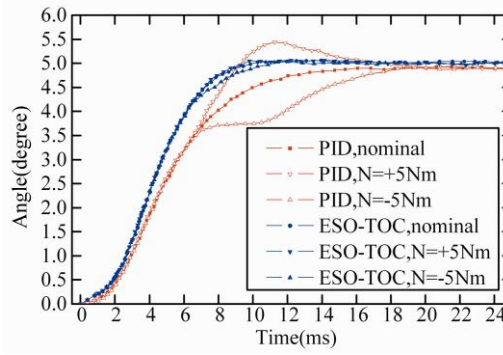


Fig. 6. Disturbance rejection.

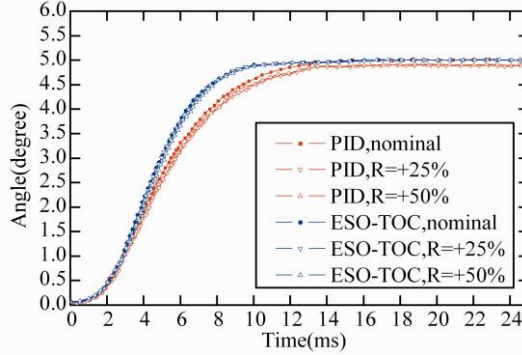


Fig. 7. Robustness to resistance variations.

It is illustrated that the ESO-TOC control converges faster than PID control. For PID control, at reference EMA's output angle θ of 5° , the EMA's output angle without apparent overshoot since the PID controller was tuned at this point. However, 1.5% and 2.5% overshoots happen at reference output angle θ of 10° and 15° , respectively. For ESO-TOC control, no overshoot happens at either reference output angle.

Disturbance Rejection. In addition, the rudder surface will bear large aerodynamic load while it's deflecting in the air, the aerodynamic load is namely the hinge moment, which can change in wide range and influence the EMA's performance. The hinge moment around the EMA aerial rudder output shaft can be obtained through Fluent simulation. In Fig.6, the ESO-TOC control rejects 5Nm moment disturbance by maintaining no overshoot while the PID control has up to 11% overshoot. When a moment disturbance of -5Nm is applied, the PID control has an apparent over damping taking a transient time of 16.5ms . Both overshoot and over damping are not allowed due to

degradation of the EMA system transient performance. It is illustrated that the performance of disturbance rejection of ESO-TOC control is better than PID control.

Robustness to Parameter Variation. The system parameters such as coil resistance R can shift from the nominal values due to increased temperature or some other factors. Fig.7 shows the simulation results that the values of R were increased by 25% and 50%, respectively. When R varies, transient times remain the same value and no overshoot happens, which indicate that both ESO- TOC control and PID control are robust to parameter variations.

Fig. 6 and Fig. 7 shows that disturbance rejection performance of the ESO-TOC is excellent since the total disturbance can be well estimated and therefore compensated.

Experimental Validation

Experiments were carried out on an EMA prototype with the same parameters given to test the performance of the proposed ESO-TOC scheme. When the flight Mach number of aircraft is fixed, the hinge moment should be assumed as an elastic load, which means hinge moment is proportional to the aerial rudder's deflection angle [7]. So a multi-channel torque characteristic simple-measurement system for the electromechanical actuator (EMA) was designed based on the elastic beam. Experimental test bench for the EMA control system is shown in Fig. 8.

Fig. 9. shows the experimental step response with angular position 5 degree, it's apparent that the experimental step response is similar to the simulated data presented in Fig.6. So the ESO-TOC controller provides a better control performance than the PID (i.e. at different angular position).

Usually the dynamic tracking ability of the system can be tested through input sinusoidal signal in different frequency. Fig.10 shows the actual response of the system, along with angular position 15 degree in frequency 5 Hz, using both controllers.

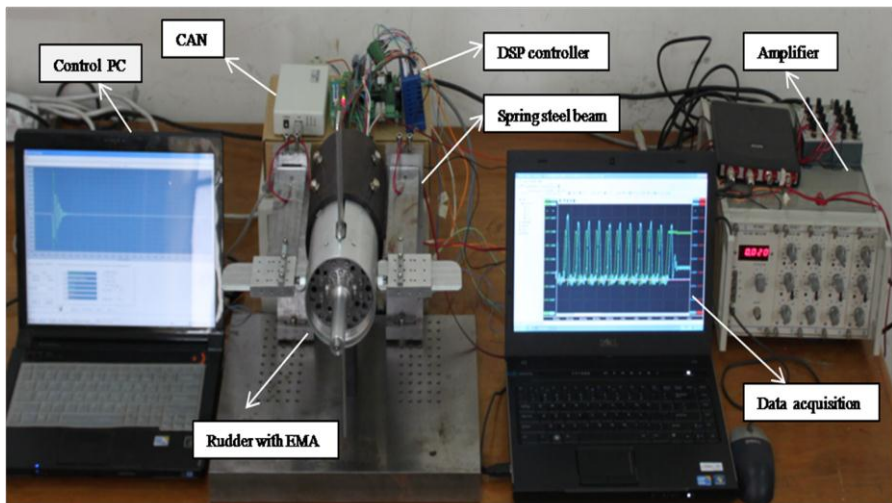


Fig. 8. Specification of experimental instruments.

It's apparent that the output amplitude of PID controller decays 16.7%, while the ESO-TOC exactly follows the input command. So the tracking performance of the total EMA system using the ESO-TOC controller is much better than using the PID controller.

Through the multi-channel torque characteristic simple-measurement system, the EMA system's bandwidth with ESO-TOC controller was obtained. According to the definition of the bandwidth, the bandwidth of the EMA system based on PID is just about 6Hz, from Fig.11 it is obviously to find that based on ESO-TOC is about 10 Hz.

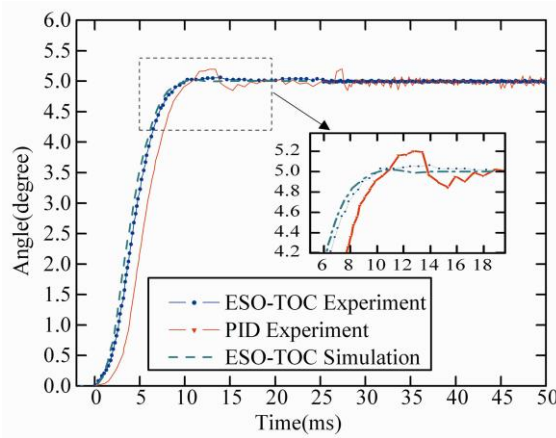


Fig. 9. Experimental step response of the ESO- TOC and PID.

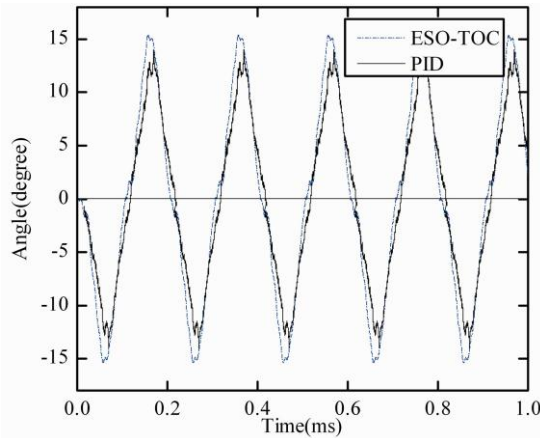


Fig. 10. Experimental response due to a 15 degree in 5Hz sine input with ESO-TOC and PID.

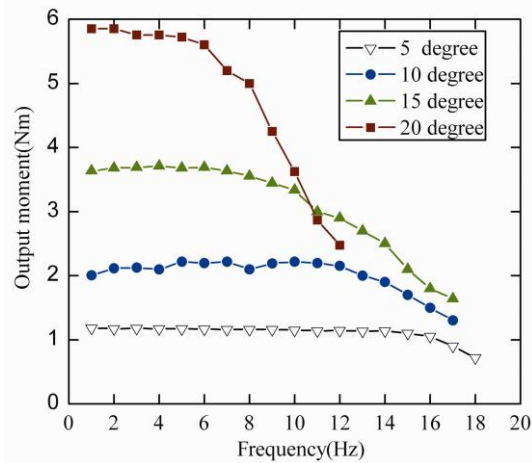


Fig. 11. The EMA frequency response due to different angular position.

As well known, a higher bandwidth results in better performance, to an extent [12]. Since the EMA system is a minor control loop within a larger vehicle control loop, a higher bandwidth allows for an increased response of the total system.

Conclusions

An ESO-TOC scheme has been proposed in this paper to achieve fast and precise angle motion control of BLDC motor driven multi channel electromechanical actuator. Combining merits of both ESO and TOC, the proposed method has the advantages of simple structure and high control performance without motion profile generators and accurate system models. Comparative simulations and experimental results indicate that the proposed ESO-TOC can achieve fast and

precise positioning performance in the presence of both model uncertainties and external disturbances.

Acknowledgements

This work was supported by the Nanjing University of Science and Technology Research Funding(NO: ZDJH02).

References

- [1] Yohan Lin and Ethan Baumann. Tests and Techniques for Characterizing and Modeling X-43A Electromechanical Actuators. NASA/TM-2008-214637.
- [2] GUO Hong, XING Wei. Development of Electromechanical Actuators. *Acta Aeronautica* , 2007,28(3), 620-627.
- [3] Jean-Francois Guery, I-Shih Chang, Toru Shimada. Solid propulsion for space applications: An updated roadmap. *Acta Astronautica*, 2010, 66(1-2), 201-219.
- [4] Douglas A.Scott, Charles L.Karr, Dale E.Schinstock. Genetic algorithm frequency-domain optimization of an anti resonant electromechanical controller. *Engineering Applications of Artificial Intelligence*, 1999, 12(2), 201-211.
- [5] Hao Lua, Yunhua Li, Chenglin Zhu. Robust synthesized control of electromechanical actuator for thrust vector system in spacecraft. *Computers and Mathematics with Applications*, 2012, 64(5), 699-708.
- [6] Gunselmann,C.and Melbert, J. Improved motion control and energy consumption for sensorless electromagnetic actuators. In 2003 IEEE 58th Vehicular Technology Conference, Orlando, USA, 6-9 October 2003, pp. 3289-3293.
- [7] CUI Ye-bing,JU Yu-tao, ZHENG Jian .Research on dual mode control for electric servo mechanism of thrust vector control. *Journal of Solid Rocket Technology*, 2012, 35(5),688-693.
- [8] B. Yao. Advanced motion control: From classical PID to nonlinear adaptive robust control, in The 11th IEEE International Workshop on Advanced Motion Control, Nagaoka, Japan, 21-24 March 2010, pp. 815-829.
- [9] Sun, F. C., Sun, Z. Q., and Zhu, Y. Y.Stable neuro-adaptive control for robots with the upper bound estimation on the neural approximation errors. *Intelligent Robotic Systems*, 26(September 1999), pp91–100.
- [10] Demirtas M. Off-line tuning of a PI speed controller for a permanent magnet brushless DC motor using DSP. *Energy Conversion and Management*.2011, 52(1), 264–273.
- [11] J. Han. From PID to active disturbance rejection control, *IEEE Trans. Indust. Electron.*, 56 (2009) 900-906.
- [12] Xia Changliang, Fang Hongwei. Permanent-Magnet Brushless DC Motor and Its Control. *Transactions of China Electrotechnical Society*, 2012, 27(3):25-34.